



Counterpropagating path-entangled photon pair sources based on simultaneous spontaneous parametric down-conversion processes of nonlinear photonic crystal

CAN YANG,¹ CHAOXIANG XI,¹ JIETAI JING,^{2,3} AND GUANGQIANG HE^{1,2,4,*}

¹State Key Laboratory of Advanced Optical Communication Systems and Networks, Department of Electronic Engineering, Shanghai Jiao Tong University, Shanghai 200240, China

²State Key Laboratory of Precision Spectroscopy, East China Normal University, Shanghai 200062, China

³Collaborative Innovation Center of Extreme Optics, Shanxi University, Taiyuan, Shanxi 030006, China

⁴National Lab of Solid State Microstructures, Nanjing University, Nanjing 210093, China

*gqhe@sjtu.edu.cn

Abstract: Ultra-bright source of entangled photons is an essential component in optical quantum information processing. Here we propose a counterpropagating path-entangled photon pair sources using a quasi-periodic modulated lithium niobate crystal. The nonlinear crystal designed by a dual-grid method, simultaneously phase-matched two spontaneous parametric down-conversion processes. Signal and idler modes have opposite propagation directions in the two spontaneous parametric down-conversion processes, which is the key to generating path-entangled photon pairs. Compared to copropagating entangled sources, the counterpropagating path-entangled sources result in a much narrower spectrum. The quantum state of the path-entanglement source is not only suited for quantum coding, but also to allow the implementation of complex quantum algorithms on a photonic chip.

© 2018 Optical Society of America under the terms of the [OSA Open Access Publishing Agreement](#)

1. Introduction

Quantum information science is a hot research field in recent years. It includes many subfields such as quantum computing [1–3], quantum cryptography [4–6], quantum dense coding [7, 8], and quantum teleportation [9–11]. Quantum communication is also an important field in quantum information science. It is theoretically safe compared to classic optical communication. For these areas of quantum information science, the essential component is an efficient and high-quality quantum entanglement source [12, 13]. Quantum entanglement is a quantum mechanical phenomenon in which the quantum states of two or more objects have to be described with reference to each other, even though the individual objects may be spatially separated [14–16]. Entangled states of quantum particles highlight the nonlocality and nonseparability of quantum mechanics [17, 18].

There are many ways to prepare entangled photon pairs. In earlier years, polarization-entangled photon pairs came from the atomic cascade [19–21]. However, the atomic cascade sources are not suitable for scalable optical quantum computation and quantum communication because they are low brightness and suffer a degrade of the polarization correlations when the two photons are not emitted back to back. Meanwhile spontaneous parametric down-conversion (SPDC) was discovered as a convenient and robust method to produce entangled photons [15]. The process of SPDC stems from the second order optical nonlinearity ($\chi^{(2)}$) in nonlinear photonic crystals. The SPDC photon pairs sources have very high purity and reasonable intensity. Today they play a key role in many quantum applications [22–24]. Besides another efficient method of generating entangled photon pairs at room temperature is through four-wave mixing (FWM) mediated by

the third order Kerr nonlinearity($\chi^{(3)}$) [25–27].

Quantum entanglement can be generated in any degree of freedom in a quantum system, such as the polarization, path, orbit-angular-momentum, frequency, or time-bin degree of freedom. According to the traditional definition, the simultaneous entanglement in multiple degrees of freedom of a quantum system is called hyperentanglement [28, 29]. In our work, we demonstrate a counterpropagating path-entangled photon pairs source using periodically-poled $LiNbO_3$ (PPLN) crystal. We employ the scheme of quasi-phase matching in the same crystal to produce counterpropagating photon pairs. Compared with dispersion engineering method to reach the phase matching of a pump mode to signal and idler modes with different propagation directions [30], the quasi-periodic modulation method of the nonlinear coefficient we used is easy to operate. And we can make crystals of any shape by this method. The entangled photon pairs from our entangled source are also easily collected in clearly opposite directions. This is not only suited for quantum coding but allows the implementation of complex quantum algorithms on a photonic chip [31].

This article is organized as follows. In Sec.2 we introduce our scheme that generates path-entangled biphoton states and the nonlinear crystals that meet our requirements are designed. In Sec.3 the SPDC Hamiltonian is introduced and we derive the Hamiltonian of the two simultaneous parametric down-conversion processes. In Sec.4 we derive the theoretical model of path-entangled two-photon states. The path-entangled states produced by our crystal are demonstrated to be maximally path-entangled bell states using theoretical analysis. The conclusions and outlooks are presented in Sec.6.

2. The path-entangled photon pairs source scheme

In this work, we report on a new scheme for generating counterpropagating path-entangled two-photon pairs in a monolithic quadratic nonlinear photonic crystal. Our scheme is formed by two simultaneous SPDC processes \mathbb{P}_A and \mathbb{P}_B . Both processes have a polarization configuration of $e \rightarrow e + e$, which is defined as the type-0 phase matching case. In process \mathbb{P}_A , the signal photons are emitted in the positive direction of the z-axis and the idler photons are emitted in the negative direction of the z-axis. The photon emission direction of processes \mathbb{P}_A and \mathbb{P}_B is exactly opposite, as schematically depicted in Fig. 1. The wavelength of the signal light is $\lambda_s = 0.776\mu m$ and the wavelength of the idler light is $\lambda_i = 0.8428\mu m$ in processes \mathbb{P}_A and \mathbb{P}_B . The light source is a 404nm continuous-wave (cw) laser. Besides, the nonlinear crystal works at a temperature of $125^\circ C$, at which the optimum conversion efficiency is obtained. For the specific frequency mode of the signal light and the idler light, i.e. the frequency listed above, the path of signal photons and the path of idler photons are uncertain but interacting in our scheme. So the path-entangled biphoton states can be collected by our entangled source.

Designing a single nonlinear crystal that simultaneously implements multiple parametric down-conversion processes is a main challenge in the scheme. According to the knowledge of nonlinear optics, the parametric down-conversion process can occur only if the momentum conservation ($\Delta k = 0$) and energy conservation conditions are met. However, the phase-matching condition (the momentum conservation) is often difficult to achieve because the refractive index of materials is an increasing function of frequency known as normal dispersion. The effective solution to the problem of phase-matching is known as quasi-phase-matching. Through quasi-periodic modulation of the nonlinear coefficient, the single nonlinear crystal can phase-match the \mathbb{P}_A and \mathbb{P}_B two processes at the same time.

We use the dual-grid method to design the required nonlinear photonic crystal [32]. This method provides a systematic algorithm for designing a crystal that can simultaneously implement different interactions with arbitrary phase-mismatch values. In our case, there are two simultaneous SPDC processes \mathbb{P}_A and \mathbb{P}_B . The phase-mismatch values shown in Fig. 2 are $\Delta k_A = k_p - k_s + k_i$ and $\Delta k_B = k_p + k_s - k_i$, respectively. The subscript p , s , and i mean pump light, signal light, and

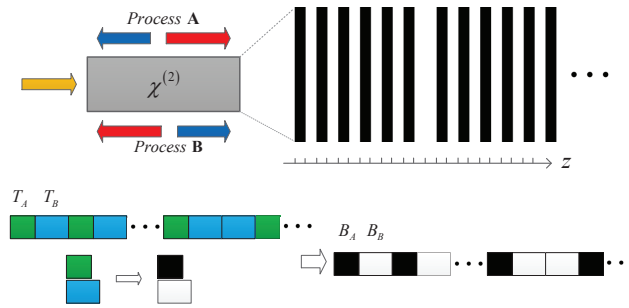


Fig. 1. The SPDC processes with counterpropagating photon pairs. The signal light is shown in red, the idler light is shown in blue, and the pump light is shown in yellow. The top right of the figure is the partial zoom of our nonlinear crystal. The lower part of the figure is a schematic diagram of the crystal design. The figure on the lower left is the one-dimensional quasi-periodic lattice composed of two basic lattice tiles. The green is marked as T_A and the blue is marked as T_B . Their lengths are $l_a = 82.4 \text{ nm}$ and $l_b = 89.29 \text{ nm}$ respectively. The lower right figure is the final nonlinear crystal. The black blocks indicate that the nonlinear coefficient is positive and the white blocks are opposite.

idler light, respectively.

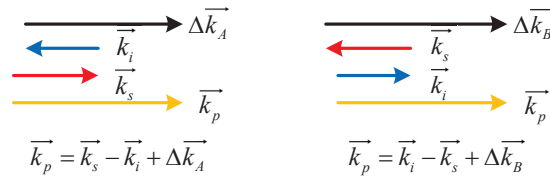


Fig. 2. The sketch of showing the momentum conservation. Δk_A and Δk_B are the phase mismatches of processes \mathbb{P}_A and \mathbb{P}_B . The left half of the picture is the phase matching condition of process A. The right half of the picture is the phase matching condition of process B.

The signal photon and idler photon are counterpropagating, which means that now the signal and idler momenta almost cancel each other and the phase-mismatch value to be accounted for by the quasi-phase-matching method is very close to the pump momentum. The phase-mismatch values of the two SPDC processes need to be compensated by the reciprocal lattice vectors (RLV) of one-dimensional quasi-periodic crystal. By applying the one-dimensional version of the dual-grid method, we obtained a one-dimensional quasi-periodic lattice, which consists of two basic lattice tiles labeled T_A and T_B . We built the nonlinear crystal from the lattice by modulating the nonlinear coefficient in the lattice tiles T_A and T_B to be positive and negative, respectively. The nonlinear coefficient modulation for the different lattice tiles can also be seen as choosing a building block for each lattice tile. These building blocks have a specific duty cycle (defined as the ratio of the positive domain length to the building length). In our crystal, the building blocks B_A and B_B are made with 100% duty cycle and 0% duty cycle, respectively. The length of the building blocks B_A and B_B is 82.4 nm and 89.29 nm respectively, which equal to the length of tiles T_A and T_B . This is illustrated in Fig. 1.

The nonlinear crystal we designed is a 40 mm long, 11.26 mm wide, and 1 mm thick 5% MgO-doped congruently grown $LiNbO_3$ crystal. The second order nonlinear coefficient $\chi^{(2)}$ of the $LiNbO_3$ crystal is modulated by the electric field poling way. We obtained the desired distribution of $\chi^{(2)}$ by applying an electric field through patterned electrodes on the crystal surface.

In addition, the input and output surfaces of the crystal were antireflection-coated for the pump, signal, and idler light to increase conversion efficiency. The crystal design process was rigorously verified by our simulation programs. The simulation parameters in the program are the same as the Ref [33, 34]. These parameters are also listed in the first paragraph of this section. The phase-mismatch values are $\Delta k_A = 35.07 \mu\text{m}^{-1}$ and $\Delta k_B = 38.003 \mu\text{m}^{-1}$ for the SPDC processes \mathbb{P}_A and \mathbb{P}_B in our scheme. The numerical simulation results show that the nonlinear crystal has the desired reciprocal lattice vectors in its reciprocal lattice. These reciprocal lattice vectors exactly achieve the momentum balance for the SPDC processes \mathbb{P}_A and \mathbb{P}_B , which means that the phase mismatches Δk_A and Δk_B are compensated by the reciprocal lattice vectors. The Fourier coefficients of the two processes are not exactly equal, but they are approximately equal to 0.4034. Figure 3 shows the Fourier coefficient at different phase mismatches. It can be seen from the figure that the expected SPDC processes \mathbb{P}_A and \mathbb{P}_B can be effectively produced and other parameter processes are suppressed.

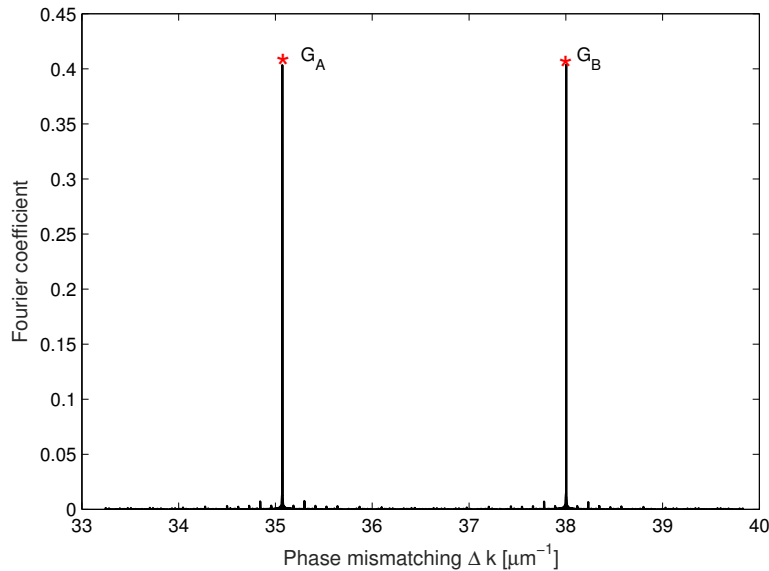


Fig. 3. The Fourier transform of our quasi-periodic lattice. The main reciprocal lattice vectors of the nonlinear photonic crystal are G_A and G_B and other vectors can be ignored.

3. The SPDC Hamiltonian

To analyze how the photon pair of signal mode and idler mode are generated, we treat the SPDC process using the Hamiltonian of the three-mode interaction including pump mode, signal mode, and idler mode. We assume the nonlinear crystal of length L centered at the origin. And all electric fields collinearly propagate along the z axis in a single spatial mode. This means that the down-converted beams are constrained to be collinear with the pump beam. We completely ignore the transverse spatial modes of the three interacting electric fields. In the experiment, this can be achieved using the pinholes.

In the interaction picture, the nonlinear interaction Hamiltonian for type-0 interaction may be taken to be

$$\hat{H}_I(t) = \varepsilon_0 \int_{-\frac{L}{2}}^{\frac{L}{2}} dz \chi^{(2)}(z) \hat{E}_p(z, t) \hat{E}_s(z, t) \hat{E}_i(z, t), \quad (1)$$

where the quantized electric fields can be divided into positive and negative frequency parts:

$$\begin{aligned}\hat{E}_m(z, t) &= \hat{E}_m^{(+)}(z, t) + \hat{E}_m^{(-)}(z, t), \\ \hat{E}_m^{(+)}(z, t) &= \hat{E}_m^{(-)\dagger}(z, t) \\ &= \int d\omega_m A_m(\omega_m) e^{j[k_m(\omega_m)z - \omega_m t]} \hat{a}_m(\omega_m).\end{aligned}\quad (2)$$

In the above formulas, $m = p, s,$ or i identifies the pump, signal, and idler waves, respectively. k_m is the wave vector of mode m . $\hat{a}_m(\omega_m)$ is the photon annihilation operator which destroys one photon with mode m at frequency ω_m . $A_m(\omega_m) = i\sqrt{\hbar\omega_m/\pi\varepsilon_0 n_m^2(\omega_{m0}) LW_0^2}$ is a slowly varying function of frequency because the bandwidth $\Delta\omega$ of the electric field of mode m is very small compared to their central frequency ω_{m0} and we only take into account the rather flat dispersion in nonlinear crystals. So $A_m(\omega_m)$ may be taken outside the integral. Note that W_0 in the expression of $A_m(\omega_m)$ labels the beam waist radius.

In our proposal, the Hamiltonian of the two simultaneous parametric down-conversion processes that satisfy type-0 phase-matching condition can be expressed as:

$$\hat{H}_f(t) \propto \varepsilon_0 \int_{-\frac{L}{2}}^{\frac{L}{2}} dz \chi^{(2)}(z) E_p^{(+)}(z, t) \hat{E}_s^{(-)}(z, t) \hat{E}_i^{(-)}(z, t) + H.c. \quad (3)$$

In the nonlinear photonic crystal, the pump, signal, and idler waves are collinear along the z axis, and the signal wave and idler wave always travel in opposite directions. So the negative parts of quantized electric fields for signal and idler waves are as follows:

$$\hat{E}_s^{(-)}(z, t) = \int d\omega_s A_s^*(\omega_s) [e^{-j[k_s(\omega_s)z - \omega_s t]} \hat{a}_{F,s}^\dagger(\omega_s) + e^{-j[-k_s(\omega_s)z - \omega_s t]} \hat{a}_{B,s}^\dagger(\omega_s)], \quad (4)$$

$$\hat{E}_i^{(-)}(z, t) = \int d\omega_i A_i^*(\omega_i) [e^{-j[k_i(\omega_i)z - \omega_i t]} \hat{a}_{F,i}^\dagger(\omega_i) + e^{-j[-k_i(\omega_i)z - \omega_i t]} \hat{a}_{B,i}^\dagger(\omega_i)]. \quad (5)$$

Because a SPDC process is very inefficient, We must use a bright pump field at the input. We consequently treat the incoming pump field as a classical field. The electric field expression of the pump wave can be replaced by the following equation:

$$\begin{aligned}E_p^{(+)}(z, t) &= E_p^{(-)*}(z, t) \\ &= A_p \int d\omega_p \alpha(\omega_p) e^{i(k_p z - \omega_p t)},\end{aligned}\quad (6)$$

where $\alpha(\omega_p)$ is the spectral distribution ranging from center frequency $\delta(\omega - \omega_c)$ for cw laser sources.

Finally, inserting Eqs. (4)-(6) into Eq. (3), we get a more detailed Hamiltonian expression for the two simultaneous SPDC processes in our scheme.

$$\begin{aligned}\hat{H}_f(t) &\propto \int_{-\frac{L}{2}}^{\frac{L}{2}} dz \iiint d\omega_p d\omega_s d\omega_i \chi^{(2)}(\omega_p, \omega_s, \omega_i, z) A_s A_i A_p \alpha(\omega_p) \\ &\times \{ e^{j\{[k_p(\omega_p) - k_s(\omega_s) + k_i(\omega_i)]z - [\omega_p - \omega_s - \omega_i]t\}} \hat{a}_{F,s}^\dagger(\omega_s) \hat{a}_{B,i}^\dagger(\omega_i) \\ &+ e^{j\{[k_p(\omega_p) + k_s(\omega_s) - k_i(\omega_i)]z - [\omega_p - \omega_s - \omega_i]t\}} \hat{a}_{F,i}^\dagger(\omega_i) \hat{a}_{B,s}^\dagger(\omega_s) \}.\end{aligned}\quad (7)$$

In our photon-entanglement source scheme, the bandwidth of signal photons and idler photons is very narrow. So the second order optical nonlinearity $\chi^{(2)}(\omega_p, \omega_s, \omega_i, z)$ change little in the narrow-band spectrum. We assume that it is only related to position in our calculation process. In fact, this assumption only affects the degree of entanglement of our path-entanglement source, but it does not affect the characteristics of path entanglement.

4. Theoretical model of path-entangled biphoton states

In this section, we derive the theoretical expression of path-entangled two-photon states on the basis of the Hamiltonian shown in the previous section. Following a standard approach in deriving two-photon states created by the SPDC process [35], we assume that the pump field is not depleted during propagation through the crystal and the interactions that are weak enough only produce two-photon states and neglect four- or higher photon states. These assumptions are also reasonable, since only a minor part of the strong pump beam is lost during the SPDC process. Consequently, we obtain the path-entangled two-photon states in the interaction picture as follows.

$$|\psi(t \rightarrow +\infty)\rangle \approx |\psi(t \rightarrow -\infty)\rangle - \frac{i}{\hbar} \int_{-\infty}^{+\infty} \hat{H}_f(t) |\psi(t \rightarrow -\infty)\rangle dt. \quad (8)$$

where $|\psi(t \rightarrow -\infty)\rangle = |0\rangle_s |0\rangle_i$. We further extended the time to plus and minus infinity in this equation, which is justified since we regard any two-photon state long after the nonlinear interaction in the medium. In the above equation, the first term is simply the initial state, which is assumed to be the vacuum state. We are interested in the second term. Hence, combining Eqs. (7) and (8) and simplifying the result, we arrive at

$$|\psi_2\rangle = T \iint d\omega_s d\omega_i \alpha(\omega_s + \omega_i) [\Gamma_A(\omega_s, \omega_i) |s, F, \omega_s\rangle |i, B, \omega_i\rangle + \Gamma_B(\omega_s, \omega_i) |s, B, \omega_s\rangle |i, F, \omega_i\rangle], \quad (9)$$

where $|s/i, F/B, \omega_s/\omega_i\rangle = \hat{a}_{s/i, F/B, \omega_s/\omega_i}^\dagger |0\rangle_{s/i}$ is the single photon state in the signal/idler mode propagating forward/backward at the frequency ω_s/ω_i . The pump distribution $\alpha(\omega_p) = \alpha(\omega_s + \omega_i)$ represents the energy conservation condition $\omega_p = \omega_s + \omega_i$. $\Gamma_A(\omega_s, \omega_i)$ and $\Gamma_B(\omega_s, \omega_i)$ are the phase-matching functions of processes A and B, respectively. They are defined as:

$$\begin{aligned} \Gamma_A(\omega_s, \omega_i) &= \int_{-\frac{L}{2}}^{\frac{L}{2}} \chi^{(2)} e^{j[k_p(\omega_s + \omega_i) - k_s(\omega_s) + k_i(\omega_i)]z} dz \\ \Gamma_B(\omega_s, \omega_i) &= \int_{-\frac{L}{2}}^{\frac{L}{2}} \chi^{(2)} e^{j[k_p(\omega_s + \omega_i) + k_s(\omega_s) - k_i(\omega_i)]z} dz \end{aligned} \quad (10)$$

The phase-matching functions result from momentum conservation condition, which is dependent on the second-order nonlinear coefficient structure and the length of the nonlinear crystal. The path-entangled two-photon states feature an intricate spectral distribution dependent on the pump distribution and the phase-matching functions.

Figure 4 also confirmed this conclusion. The phase-matching functions of the SPDC with counterpropagating signal and idler photons are discrete in our nonlinear crystal. This is due to the quasi-periodic modulation of the second-order nonlinear coefficient of our lithium niobate crystal. Figure 3 shows the Fourier transform of our quasi-periodic lattice. This Fourier transform spectrum is discrete, which means that the reciprocal lattice vectors of the nonlinear photonic crystal are discrete and the Fourier coefficients are mainly concentrated on the two reciprocal lattice vectors we design. So only some discrete parametric processes implement quasi-phase matching in our quasi-periodic modulation crystal. The phase-matching amplitude therefore also exhibits discrete features. In the case of a cw-laser source with a narrow linewidth, the joint-spectral amplitude distribution of pump spectral distribution and phase-matching spectral distribution is formed under conditions of the energy conservation and momentum conservation. We can see from the figures that the parametric down-conservation processes A and B occur simultaneously and other processes are completely suppressed. This result also shows that

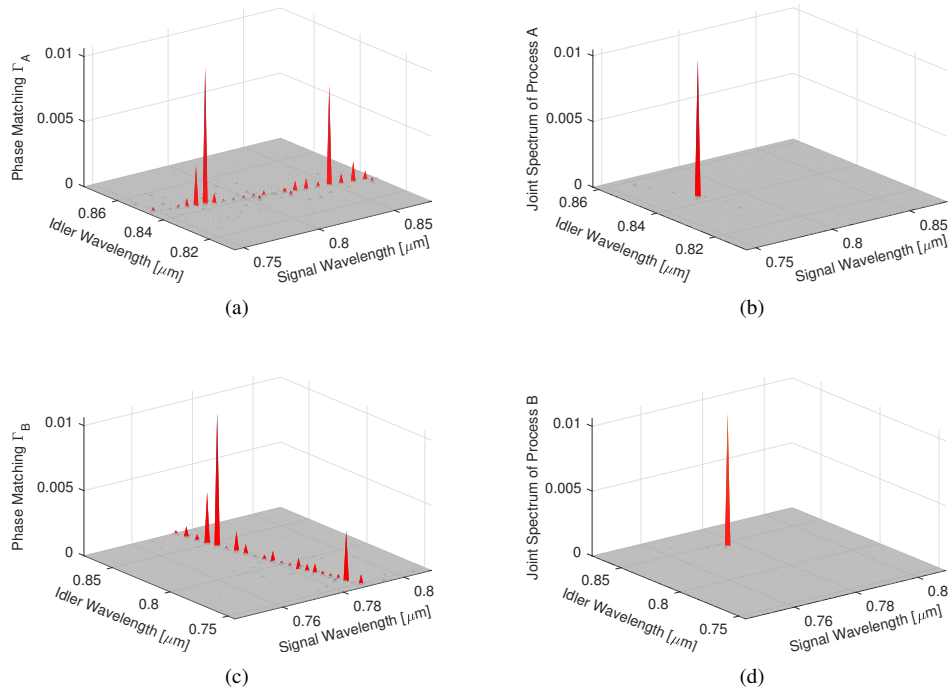


Fig. 4. The spectrum distribution of simultaneous spontaneous parametric processes A and B. (a), (c) phase-matching functions of process A and process B, respectively. (b), (d) joint-spectral amplitude distribution of process A and process B, respectively. The joint-spectral amplitude of process A is determined by the continuous-wave laser source and its phase matching function Γ_A in the first row. The process B is the same in the second row.

our scheme is feasible. Note that the joint-spectral distribution functions of the simultaneous parameter processes A and B describe the spectral properties of the generated photon pairs.

To generate a maximally path-entangled two-photon state, we must have the same nonlinear efficiency along with modal and spectral indistinguishability for processes A and B [30]. For modal indistinguishability, this can be guaranteed because the forward propagation and backward propagation counterparts of the signal and idler modes in a single crystal are identical. As for spectral indistinguishability, We can verify it through the simulation results in Fig. 4. The nonlinear efficiencies of processes A and B are defined as $\iint d\omega_s d\omega_i \alpha(\omega_s + \omega_i) \Gamma_A(\omega_s, \omega_i)$ and $\iint d\omega_s d\omega_i \alpha(\omega_s + \omega_i) \Gamma_B(\omega_s, \omega_i)$, respectively, which depend on the Fourier transform of our quasi-periodic lattice. The nonlinear efficiency is proportional to the Fourier transform coefficient and pump distribution. So the value of joint-spectral distribution in the Fig. 4 is also proportional to the nonlinear efficiency. From the joint-spectral distribution, the nonlinear efficiencies of processes A and B are very high, while the nonlinear efficiencies of other nonlinear processes are almost zero in our scheme. The nonlinear efficiencies of processes A and B are approximately equal. To further illustrate the nonlinear efficiency value, we respectively plot the nonlinear efficiencies of the processes A and B as the function of crystal length.

According to the definition of nonlinear efficiencies of processes A and B above, nonlinear efficiency is related to the length of the crystal. In Fig. 5, we plot the nonlinear efficiency values at different position in the crystal in order to determine whether the nonlinear efficiencies of processes A and B are equal. As can be seen from the figure, nonlinear efficiency gradually

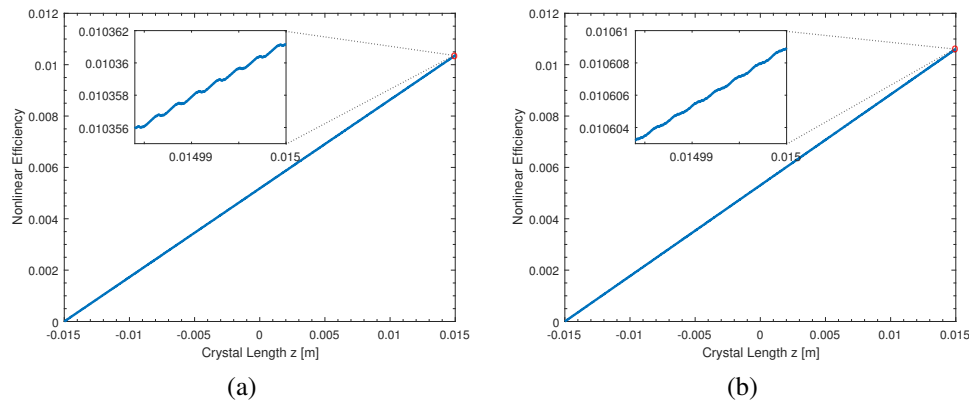


Fig. 5. The nonlinear efficiencies of processes A and B as the function of crystal length. (a) process A. (b) process B. From the inserted figures, the nonlinear efficiency fluctuates with distance but the overall trend is increased. The effective difference between the nonlinear efficiencies of processes A and B is only one percent.

becomes larger as the crystal length increases. And the nonlinear efficiency periodically increases by a short distance, as shown in the insert. This is due to the quasi-periodic modulation of the second-order nonlinear coefficient in nonlinear crystal. Besides the nonlinear efficiencies of the two processes are different, but their difference is extremely small. One of the reasons for this subtle difference is the quantization in the simulations.

5. Discussion

Our path-entanglement source allows full control over the path degree of freedom of entangled biphoton states compared to existing photon entanglement sources [36]. An additional degree of freedom for creating entanglement in monolithic crystals is developed. And the path-entangled states of our sources are easy to be collected because the propagating direction of signal and idler modes are opposite. Different from other polarization entanglement sources based on quasi-phase matching of SPDC processes [37, 38], the path-entanglement photon pairs from our source are easier to be detected. In other words, the detection system does not have to be equipped with many polarizers to rotate the photon polarization. Counterpropagating configurations in our scheme allow the splitting of the signal and idler photons from each other. So our entanglement scheme effectively reduces the complexity of the receiving system, which facilitates on-chip integration of path-entanglement applications.

In this work, the spatial modes of the down converted beams from the crystal can encode information, which is an effective way to distribute quantum keys. Our entangled sources can also be used in some quantum information applications, such as heralded single-photon source and quantum teleportation [39]. The heralded single-photon can be directly generated and easily collected from a quasi-periodic modulated nonlinear crystal. Besides other degrees of freedom like polarization and orbital angular momentum can also be manipulated inside the same crystal, which will facilitate the preparation of hyper-entanglement with multiple degrees of freedom. Considering the state-of-the-art domain-engineered technique, our path-entanglement source in bulk can be developed into on-chip integrated quantum entanglement source. The inherent stability of integrated optics make on-chip integrated path-entanglement source be a promising choice for quantum information application which require circuits that are stable, high-fidelity and highly reconfigurable.

6. Conclusion

In summary, we propose an effective entangled preparation scheme, which prepares counter-propagating path-entangled biphoton quantum states in a quasi-periodic modulated nonlinear photonic crystal. We design the quasi-periodic modulated $LiNbO_3$ crystals by universal dual-grid method. The $LiNbO_3$ crystal is a common second-order nonlinear material. It can be used to generate SPDC processes, which is the basis of our path-entanglement source. The dual-grid method we used is a general algorithm for designing the quasi-periodic modulated nonlinear photonic crystals. Besides we discuss the theory of SPDC process in the two-photon picture. A photon from the incident pump field spontaneously decays into two photons labelled signal and idler in a second-order nonlinear photonic crystal. This process is described by the interaction Hamiltonian for nondegenerate three-wave mixing in a lossless nonlinear dielectric medium. We also carefully derive the expression of counterpropagating path-entangled biphoton states and get the joint-spectral-amplitude functions. Joint-spectral-amplitude functions show the spectral characteristics of path-entangled photon pairs.

For now, our path-entangled source is a stable, efficient and convenient device for creating path-entangled biphoton states. Quasi-periodic modulation of second order optical nonlinearity ($\chi^{(2)}$) of nonlinear photonic crystals is a versatile and effective method to achieve multiple simultaneous parametric processes. We can achieve a variety of photon entanglement sources based on the simultaneous SPDC processes.

Funding

National Natural Science Foundation of China (61475099), Program of State Key Laboratory of Quantum Optics and Quantum Optics Devices (KF201701).

Acknowledgments

The authors thank the anonymous reviewers for their helpful suggestions and comments.

References

1. M. A. Nielsen, and I. L. Chuang, *Quantum Computation and Quantum Information* (Cambridge University, 2011).
2. E. Knill, R. Laflamme, and G. J. Milburn, "A scheme for efficient quantum computation with linear optics," *Nature* **409**, 46–52 (2001).
3. W. -B. Gao, P. Xu, X. -C. Yao, O. Gühne, A. Cabello, C. -Y. Lu, C. -Z. Peng, Z. -B. Chen, and J. -W. Pan, "Experimental realization of a controlled-NOT gate with four-photon six-qubit cluster states," *Phys. Rev. Lett.* **104**, 020501 (2010).
4. H. -K. Lo, M. Curty, and B. Qi, "Measurement-device-independent quantum key distribution," *Phys. Rev. Lett.* **108**, 130503 (2012).
5. H. Zhang, J. Fang, and G. He, "Improving the performance of the four-state continuous-variable quantum key distribution by using optical amplifiers," *Phys. Rev. A* **86**, 022338 (2012).
6. X. Wang, W. Liu, P. Wang, and Y. Li, "Experimental study on all-fiber-based unidimensional continuous-variable quantum key distribution," *Phys. Rev. A* **95**, 062330 (2017).
7. X. Li, Q. Pan, J. Jing, J. Zhang, C. Xie, and K. Peng, "Quantum dense coding exploiting a bright Einstein-Podolsky-Rosen beam," *Phys. Rev. Lett.* **88**, 047904 (2002).
8. J. Zhang, and K. Peng, "Quantum teleportation and dense coding by means of bright amplitude-squeezed light and direct measurement of a Bell state," *Phys. Rev. A* **62**, 064302 (2000).
9. S. Pirandola, J. Eisert, C. Weedbrook, A. Furusawa, and S. L. Braunstein, "Advances in quantum teleportation," *Nat. Photonics* **9**, 641–652 (2015).
10. J. Yin, J. -G. Ren, H. Lu, Y. Cao, H. -L. Yong, Y. -P. Wu, C. Liu, S. -K. Liao, F. Zhou, Y. Jiang, X. -D. Cai, P. Xu, G. -S. Pan, J. -J. Jia, Y. -M. Huang, H. Yin, J. -Y. Wang, Y. -A. Chen, C. -Z. Peng, and J. -W. Pan "Quantum teleportation and entanglement distribution over 100-kilometre free-space channels," *Nature* **488**, 185–188 (2012).
11. G. He, J. Zhang, J. Zhu, and G. Zeng, "Continuous-variable quantum teleportation in bosonic structured environments," *Phys. Rev. A* **84**, 034305 (2011).
12. J. Jing, J. Zhang, Y. Yan, F. Zhao, C. Xie, and K. Peng, "Experimental demonstration of tripartite entanglement and controlled dense coding for continuous variables," *Phys. Rev. Lett.* **90**, 167903 (2003).
13. X. Jia, Z. Yan, Z. Duan, X. Su, H. Wang, C. Xie, and K. Peng, "Experimental realization of three-color entanglement at optical fiber communication and atomic storage wavelengths," *Phys. Rev. Lett.* **109**, 253604 (2012).

14. A. Einstein, B. Podolsky, and N. Rosen, "Can quantum-mechanical description of physical reality be considered complete?," *Phys. Rev.* **47**, 777–780 (1935).
15. P. G. Kwiat, K. Mattle, H. Weinfurter, A. Zeilinger, A. V. Sergienko, and Y. Shih, "New high-intensity source of polarization-entangled photon pairs," *Phys. Rev. Lett.* **75**, 4337 (1995).
16. X. -C. Yao, T. -X. Wang, P. Xu, H. Lu, G. -S. Pan, X. -H. Bao, C. -Z. Peng, C. -Y. Lu, Y. -A. Chen, and J. -W. Pan, "Observation of eight-photon entanglement," *Nat. Photonics* **6**, 225–228 (2012).
17. B. Hensen, H. Bernien, A. E. Dréau, A. Reiserer, N. Kalb, M. S. Blok, J. Ruitenberg, R. F. L. Vermeulen, R. N. Schouten, C. Abellán, W. Amaya, V. Pruneri, M. W. Mitchell, M. Markham, D. J. Twitchen, D. Elkouss, S. Wehner, T. H. Taminiiau, and R. Hanson, "Loophole-free Bell inequality violation using electron spins separated by 1.3 kilometres," *Nature* **526**, 682–686 (2015).
18. M. A. Rowe, D. Kielpinski, V. Meyer, C. A. Sackett, W. M. Itano, C. Monroe, and D. J. Wineland, "Experimental violation of a Bell's inequality with efficient detection," *Nature* **409**, 791–794 (2001).
19. J. F. Clauser, and A. Shimony, "Bell's theorem: experimental tests and implications," *Reports on Prog. Phys.* **41**, 1881–1927 (1978).
20. A. Aspect, P. Grangier, and G. Roger, "Experimental tests of realistic local theories via Bell's theorem," *Phys. Rev. Lett.* **47**, 460 (1981).
21. A. Aspect, P. Grangier, and G. Roger, "Experimental realization of Einstein-Podolsky-Rosen-Bohm gedankenexperiment: a new violation of Bell's inequalities," *Phys. Rev. Lett.* **49**, 91 (1982).
22. J. -W. Pan, Z. -B. Chen, C. -Y. Lu, H. Weinfurter, A. Zeilinger, and M. Żukowski, "Multiphoton entanglement and interferometry," *Rev. Mod. Phys.* **84**, 777–838 (2008).
23. J. C. F. Matthews, A. Politi, A. Stefanov, and J. L. O'Brien, "Manipulation of multiphoton entanglement in waveguide quantum circuits," *Nat. Photonics* **3**, 346–350 (2009).
24. A. Peruzzo, M. Lobino, J. C. F. Matthews, N. Matsuda, A. Politi, K. Poulios, X. -Q. Zhou, Y. Lahini, N. Ismail, K. W. Źurhoff, Y. Bromberg, Y. Silberberg, M. G. Thompson, and J. L. O'Brien, "Quantum walks of correlated photons," *Science* **329**, 1500–1503 (2010).
25. K. F. Lee, J. Chen, C. Liang, X. Li, P. L. Voss, and P. Kumar, "Generation of high-purity telecom-band entangled photon pairs in dispersion-shifted fiber," *Opt. Lett.* **31**, 1905–1907 (2006).
26. J. Fan, M. D. Eisaman, and A. Migdall, "Quantum state tomography of a fiber-based source of polarization-entangled photon pairs," *Opt. Express* **15**, 18339–18344 (2007).
27. J. W. Silverstone, D. Bonneau, K. Ohira, N. Suzuki, H. Yoshida, N. Iizuka, M. Ezaki, C. M. Natarajan, M. G. Tanner, R. H. Hadfield, V. Zwiller, G. D. Marshall, J. G. Rarity, J. L. O'Brien, and M. G. Thompson, "On-chip quantum interference between silicon photon-pair sources," *Nat. Photonics* **8**, 104–108 (2014).
28. J. T. Barreiro, N. K. Langford, N. A. Peters, and P. G. Kwiat, "Generation of hyperentangled photon pairs," *Phys. Rev. Lett.* **95**, 260501 (2005).
29. F. -G. Deng, B. -C. Ren, and X. -H. Li, "Quantum hyperentanglement and its applications in quantum information processing," *Sci. Bull.* **62**, 46–68 (2017).
30. S. Saravi, T. Pertsch, and F. Setzpfandt, "Generation of counterpropagating path-entangled photon pairs in a single periodic waveguide," *Phys. Rev. Lett.* **118**, 183603 (2017).
31. A. S. Solntsev, and A. A. Sukhorukov, "Path-entangled photon sources on nonlinear chips," *Rev. Phys.* **2**, 19–31 (2017).
32. R. Lifshitz, A. Arie, and A. Bahabad, "Photonic quasicrystals for nonlinear optical frequency conversion," *Phys. Rev. Lett.* **95**, 133901 (2005).
33. S. Sharabi, G. Porat, and A. Arie, "Improved idler beam quality via simultaneous parametric oscillation and signal-to-idler conversion," *Opt. Lett.* **39**, 2152–2155 (2014).
34. G. Porat, O. Gayer, and A. Arie, "Simultaneous parametric oscillation and signal-to-idler conversion for efficient downconversion," *Opt. Lett.* **35**, 1401–1403 (2010).
35. W. P. Grice, and I. A. Walmsley, "Spectral information and distinguishability in type-II down-conversion with a broadband pump," *Phys. Rev. A* **56**, 1627 (1997).
36. F. Laudenbach, S. Kalista, M. Hentschel, P. Walther, and H. H. Āijbel, "A novel single-crystal & single-pass source for polarisation- and colour-entangled photon pairs," *Sci. Reports* **7**, 7235 (2017).
37. T. Suhara, G. Nakaya, J. Kawashima, and M. Fujimura, "Quasi-phase-matched waveguide devices for generation of postselection-free polarization-entangled twin photons," *IEEE Photonics Technol. Lett.* **21**, 1096–1098 (2009).
38. H. Herrmann, X. Yang, A. Thomas, A. Poppe, W. Sohler, and C. Silberhorn, "Post-selection free, integrated optical source of non-degenerate, polarization entangled photon pairs," *Opt. Express* **21**, 27981–27991 (2013).
39. G. Bj. Āürk, A. Laghaout, and U. L. Andersen, "Deterministic teleportation using single-photon entanglement as a resource," *Phys. Rev. A* **85**, 022316 (2012).